Chemistry Europe
European Chemical Societies Publishing

WILEY VCH

Excellence in Chemistry Research

Announcing our new flagship journal

- Gold Open Access
- Publishing charges waived
- Preprints welcome
- Edited by active scientists

Meet the Editors of *ChemistryEurope*

Luisa De Cola
Università degli Studi di Milano Statale, Italy

Ive Hermans
University of Wisconsin-Madison, USA

Ken Tanaka
Tokyo Institute of Technology, Japan

ChemistrySelect

Research Article
doi.org/10.1002/slct.202300797

Chemistry Europe
European Chemical Societies Publishing

www.chemistryselect.org

Controlling the Self-Assembly of Hierarchical PS-*b*-P4VP Structures Prepared by Dip-Coating and Emulsion Breath Figure Techniques

Hoang M. Nguyen,[a] Ariane V. Mader,[b] Swarnalok De,[a] Fevzihan Basarir,[a] and Jaana Vapaavuori*[a]

The breath figure (BF) method is a common laboratory-scale pathway for fabricating porous structures. The emulsion BF approach, one of the BF variations, has attracted increasing attention since it bypasses the high humidity requirement, which is characteristic for the conventional BF method. In this paper, we used the emulsion BF technique with PS-*b*-P4VP block copolymer (BCP) and SiO_2 nanoparticles (NPs) as the stabilizers for water droplets. We combined this with the dip-coating technique to obtain a hierarchical structure consisting of BF pores and BCP nanodomains. By altering the dip-coating speeds and the NPs' surface wetting properties and size, the average diameters of BF pores could be controlled. Notably, we were able to achieve both nano and microscale BF pores in the network. The effect of NPs for stabilization and dip-coating parameters on BF pores and BCP nanodomains formation was established, extending the comprehension of this underdeveloped subject.

Introduction

In the nature around us, hierarchical structures are widely encountered and their construction commonly relies on natural self-assembly processes.[1] Inspired by nature, synthetic materials with multiple levels of hierarchy are of particular interest due to their limitless possibilities to combine different architectures and functionalities to create a single unique material.[2] Over the last decade, those materials have proven their notable performance in the fields of photonics,[3–5] energy storage,[6–8] membrane filtration,[9,10] sensing,[11–13] and catalysis.[14–16] Despite their great potential, the ability to precisely control the self-assembly of building blocks over multiple length scales, along with the development of a facile, cost-effective, and industrially applicable method, remain challenges.[17,18]

The breath figure (BF) method, coined by François *et al.* in 1994,[19] has been utilized to produce microporous films for the past 25 years.[20] In a conventional BF process, a polymer solution is cast onto a substrate exposed to a humid atmosphere. The evaporation of organic solvent leads to the cooling of the solution surface, on which water droplets thus condense and self-organize. Finally, the complete evaporation of both the solvent and the water results in a solid porous film.[21] By selecting appropriate BF materials, substrate wettability, solvent, and humidity levels,[20–22] this technique offers a versatile control over the pore size and pore arrangement. Through variation of the applied materials, these honeycomb structured films can produce functionalities, such as antibacteriality,[23] microfluidics, cell culture substrates,[24] and gravimetric water–oil separation.[25]

For the traditional BF method, the use of a humid environment is indispensable, and to achieve a regular BF array, high humidity levels of at least 50% relative humidity (RH) are needed.[21,22] In addition to posing a significant challenge to industrial scalability, such precise control tends to be laborious even in the laboratory environment, since it often requires complicated setups. On the other hand, the emulsion technique – a variation of the original BF method – offers a straightforward and single-step method of producing ordered microporous structures.[22]

In the emulsion approach of creating breath figures, water is directly added to an immiscible organic solvent to form a water-in-oil emulsion.[22] Thus, no atmospheric humidity is needed to create water droplets. The BF emulsion method has been applied to successfully fabricate polystyrene-*b*-poly(2-hydroxyethyl methacrylate),[26] polystyrene-*b*-poly(N-isopropylacrylamide),[27] polystyrene and poly(methyl methacrylate),[28,29] poly(styrene-butyl acrylate-acrylic acid) latex,[30] polyoxometalates inorganic cluster,[31] porous cellulose,[32] and protein[33] films. Polymers are commonly used due to their ability to form stable thin films and their often-limited water solubility, which is effectively stabilizing the water droplets. Among the broad spectrum of polymeric materials, amphiphilic block copolymers (BCP) can form highly ordered BF arrays through conventional BF method, as they can act as stabilizing surfactants. More importantly, the intriguing self-assembly of BCP has been utilized to create a synergistic network of BF microporous structures and BCP nanodomains.[34–38] However, in all of these works, in order to manipulate the shape and the order of such nanodomains, intricate and time-consuming set-ups, such as solvent anneal-

[a] *H. M. Nguyen, Dr. S. De, Dr. F. Basarir, Prof. J. Vapaavuori*
Department of Chemistry and Materials Science, Aalto University, Espoo 02150, Finland
E-mail: jaana.vapaavuori@aalto.fi
[b] *A. V. Mader*
AMOLF, Science Park 104, Amsterdam 1098 XG, Netherlands

Supporting information for this article is available on the WWW under https://doi.org/10.1002/slct.202300797

ing and thermal annealing, are often required, which can introduce defects or unintentionally alter the BF pores. Nanoparticles are also attractive for stabilizing water droplets, owing to their additional unique catalytic, optical, and electrical functionalities that can be introduced with them. Especially in the BF emulsion technique, silica NPs have been commonly used due to their versatility of surface modification.[39–41] Nevertheless, the number of reported porous materials obtained by using the emulsion technique is much lower in comparison to that using the conventional BF method and the experimental parameters governing the pore formation are not yet well-understood.

Among the various thin film deposition techniques, dip-coating stands out as a facile, resource-efficient, and industrially scalable method.[42] During a common dip-coating procedure, a substrate is immersed in a coating solution, and then withdrawn vertically at a chosen speed. After the complete evaporation of solvent on the substrate, a thin film is usually obtained within seconds to minutes after withdrawal. The thickness of the film is closely associated with the speed.[42] At slow speeds, the capillary regime, the lengthened capillary feeding and slow evaporation rate dominate the process, hence a thicker film is produced the slower it is withdrawn. At high withdrawal rates, the draining regime, the draining force of the solution predominantly takes place, resulting in a film thickness obeying the Landau-Levich equation.[43] In this regime, a thicker film can be obtained by faster withdrawal. An intermediate regime is found between the two other regimes. Here, the governing and opposing forces are roughly equal, which leads to the creation of the thinnest film. Once the regimes for a specific system have been identified, thickness control with precision in the nanometer range is possible.[42] In addition, the dried film is exposed to a solvent vapor layer during the withdrawal step, effectively creating solvent annealing conditions and making further post-processing steps obsolete.

While few works have already applied dip-coating for the BF emulsion technique, investigations about the relationship between dip-coating speed and the BF were neglected,[29,44] or only focused on the high speed regime (*e.g.*, faster than 100 mm/min).[45] Such high dip-coating speeds are likely to be located in draining regime, thus leaving the interesting interplay of different dip-coating regimes unexploited. In this article, we produced a hierarchical BF microstructure – BCP nanopattern network at ambient humidity and studied the effect of dip-coating speeds and solution composition on the structural formation. To our knowledge, this is the first report on such a hierarchical structure prepared by the BF emulsion technique. By varying the dip-coating speeds and the stabilizing nanoparticle modification and sizes, we were able to obtain a hierarchical network containing different BF pore sizes ranging from 150 to 500 nm on average, and BCP nanostructures of stripe and dot patterns in a ten-fold smaller size range. Unprecedentedly, another network of micrometer-sized BF pores was also created simultaneously with the nanoscale BF pores, forming a third distinctive level of hierarchy. Overall, the underlying processes leading to both the BF pores and the BCP nanostructure evolution were discussed with regard to dip-coating and emulsion parameters.

Results and Discussions

Material Choices

The objective of this research was to investigate the effects of dip-coating speed and emulsion composition on the morphological evolution of BFs. For this purpose, as illustrated in Figure 1, BF films were created by dip-coating a substrate into

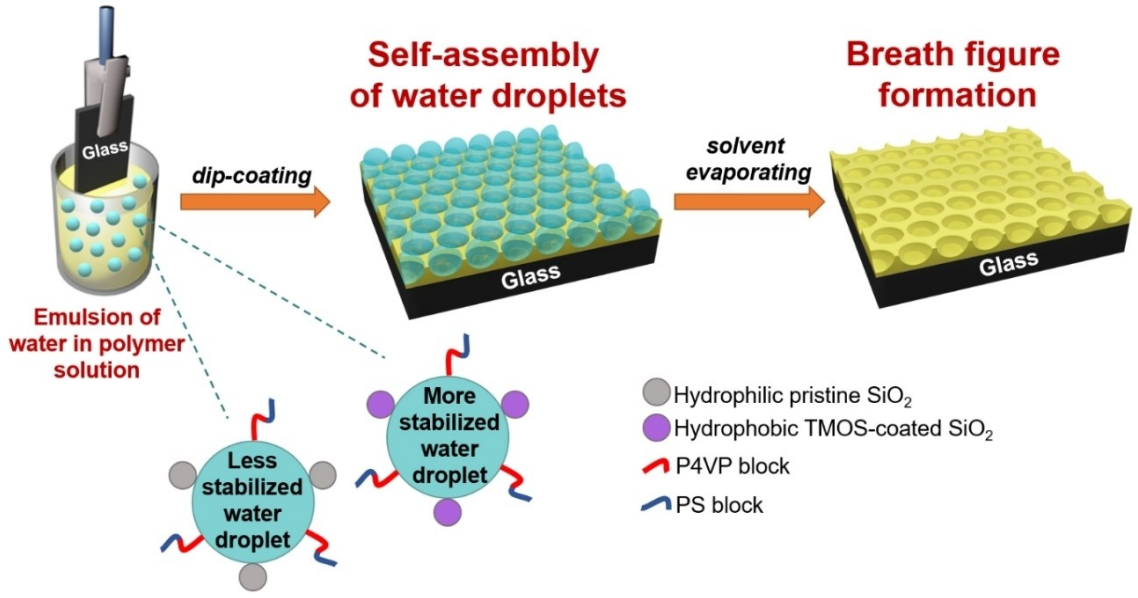

Figure 1. Schematic illustration of the fabrication of BF.

an emulsion consisting of water as the dispersed and PS-*b*-P4VP in chloroform as the continuous phase. PS-*b*-P4VP is an amphiphilic BCP, which has been extensively studied in the context of conventional BF fabrication.[46–49] The PS block is soluble in a wide range of organic solvents and the P4VP block can stabilize the water droplets during the BF formation by hydrophilic interactions. However, in our case, a stable emulsion could not be achieved solely by the P4VP block, indicated by phase separation between water and chloroform, resulting in a non-continuous BF film (Figure S2a).

The BCP should exhibit amphiphilicity in both dispersed and continuous phase simultaneously to create a stable emulsion,[50] while in our experiment both the PS and P4VP blocks are soluble in chloroform. Therefore, pristine silica nanoparticles (SiO_2 NPs) which are natively hydrophilic,[51] were added as stabilizers, ensuring smooth dip-coated BF films. This ensured that the emulsion retained a homogenous opaque white colour for at least 24 hours, indicating the improved stability (Figure S2b). Inspired by the work of Kaptay *et al.*,[52] in which the water-in-oil emulsion was reported to be the most stabilized if the contact angle between solid particle and water phase ranged from 90° to 165°, we further modified the hydrophilic pristine SiO_2 NPs with TMOS (for details, please refer to the experimental section). FTIR data of the altered SiO_2 particles proved the modification successful (Figure S3), as the presence of –CH stretching vibrations of alkyl groups at 2901 and 2983 cm^{-1} was observed after the modification.[51]

The dip-coating withdrawal speed was varied from 1 to 100 mm/min, and the concentration of water, BCP, and SiO_2 NPs, chosen based on the optimization done in our previous work,[53] was kept constant throughout the experiment. After both the organic solvent and the water droplets evaporated completely, an ordered breath figure array was formed. In the following, the impacts of SiO_2 NPs and dip-coating speed on the morphology of the formed BF, and finally the evolution of the BCP nanostructure within the BF network, will be discussed.

Effect of Surface Wettability of NPs and Dip-Coating Speeds

In order to study the morphological evolution of BFs, a series of SEM images demonstrating the morphologies of the films was attained. Figure 2 shows the BF films dip-coated from the emulsion stabilized with unmodified hydrophilic and modified hydrophobic 20 nm SiO_2 NPs. The dimensions of the pores, derived from the images with the help of a Python-based algorithm, are summarized in Figure 3. The porous structure was seen for all the films regardless of the solution composition and the withdrawal speed. When the unmodified SiO_2 NPs were used, at the lowest dip-coating speed of 1 mm/min, the BF structure spanned the entire substrate with pores of ca. 330 nm diameters (Figure $2a_1$). A high degree of deviation in pore size was observed, as indicated by a standard deviation (SD) value of 314 nm. The pattern created at 10 mm/min also spanned the entire film and had a more uniform pore diameter (358 ± 154 nm) (Figure $2a_2$). At higher speed regimes ranging from 50 to 100 mm/min, the average pore diameters increased to ca. 500 nm (Figure $2a_3$–$2a_5$) with a similar degree of monodispersity as that of the 10 mm/min sample. Notably, the films coated at speeds faster than 50 mm/min seemed not to wet the substrate fully, as illustrated by the unpatterned regions amid the porous structures. This type of defect likely originated from the collapse of insufficiently stabilized droplets, which then led to the formation of a thin water film.

When SiO_2 NPs were hydrophobically modified, intriguingly, at the lowest speed of 1 mm/min the pores were much smaller, with diameters of 152 nm on average, and their size distribution was narrow (Figure $2b_1$). When higher speeds of 10–100 mm/min were applied (Figure $2b_2$–$2b_5$), the overall average pore diameter increased to 358–403 nm but was still smaller in

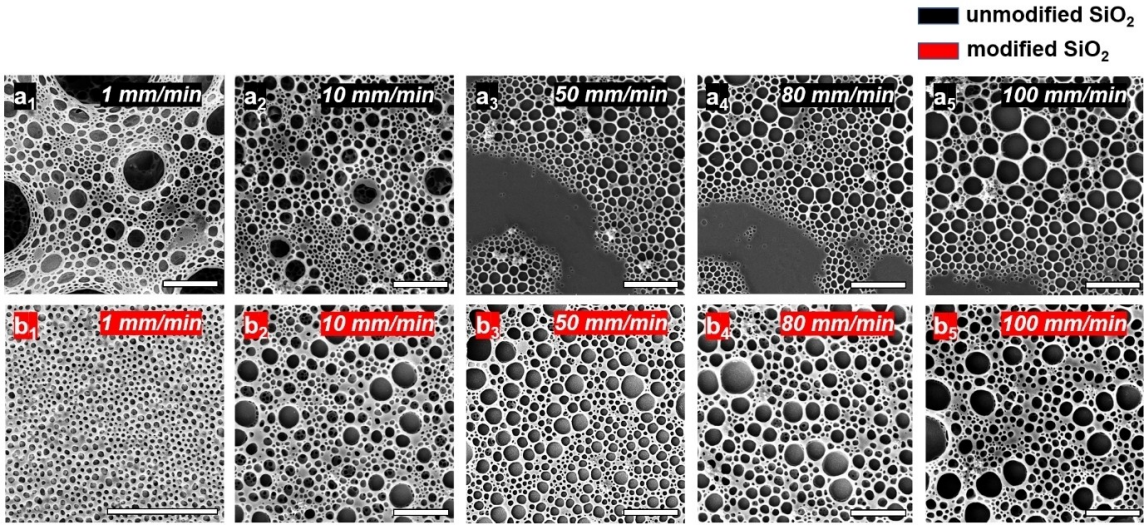

Figure 2. SEM images of the BF films dip-coated from emulsions containing (a_1–a_5) bare and (b_1–b_5) modified 20 nm SiO_2 NPs at various withdrawal speeds. The scale bars are 5 μm.

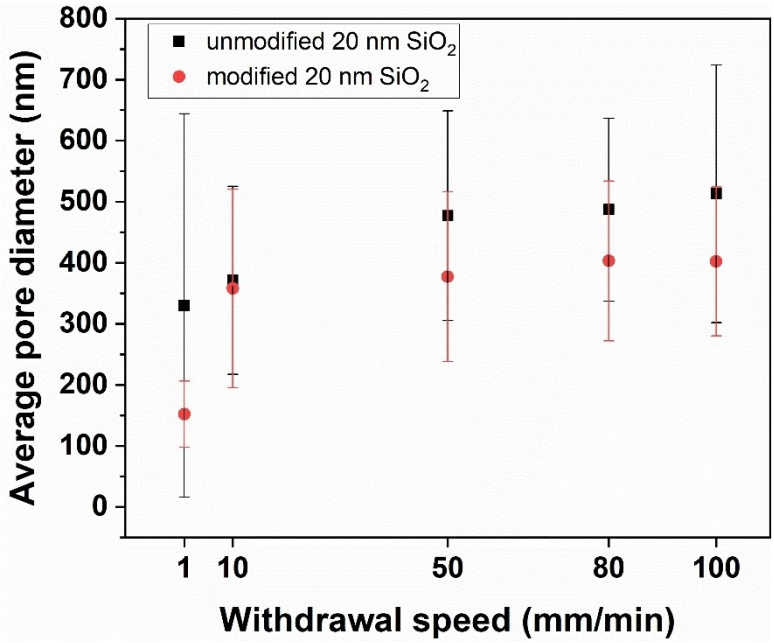

Figure 3. Relationship between withdrawal speed and average BF pore diameter of the films dip-coated from unmodified (black square) and modified 20 nm SiO_2 NPs (red circle).

comparison to that obtained with unmodified SiO_2 NPs over the same dip-coating speed range. Furthermore, the BF structure spanned the entire substrate at all speeds. These findings confirm that hydrophobic SiO_2 NPs are more effective at stabilizing the water droplets than the hydrophilic ones.

Dynamic light scattering (DLS) was conducted to examine the stability of the emulsions before the dip-coating process (Figure S4). The size distribution of water droplets capped by modified SiO_2 showed one prominent peak at ca. 371 nm, while in the case of bare SiO_2, a bimodal size distribution peaking at ca. 484 nm and 2025 nm was observed, demonstrating droplet coalescence. The DLS distribution data of droplets was in good agreement with the pore size values derived from SEM and further consolidates that the TMOS modification benefited the stabilization of the BF emulsion.

Regarding the effect of withdrawal speed on the BF pore size, it appears plausible that at lower withdrawal speed the pores would be larger due to the longer retention time for the droplets to grow through coalescence or other mechanisms. Our results suggest the contrary, as the smallest pore size of 152 nm was obtained at the lowest withdrawal speed in the case of modified SiO_2 NPs (Figure 2b$_1$). This speed is part of the capillary regime, where the thickest films are usually achieved. Indeed, the cross-sectional SEM images reveals that a 25 μm-thick multilayer BF structure was present when withdrawing at 1 mm/min, while films withdrawn at 10–100 mm/min were much thinner, namely 0.4–2 μm (Figure 4).

In order to establish a link between dip-coating speed and BF pattern formation, the underlying forces behind both dip-coating regimes and types of BF structures should be considered. In the conventional BF method, the order of water

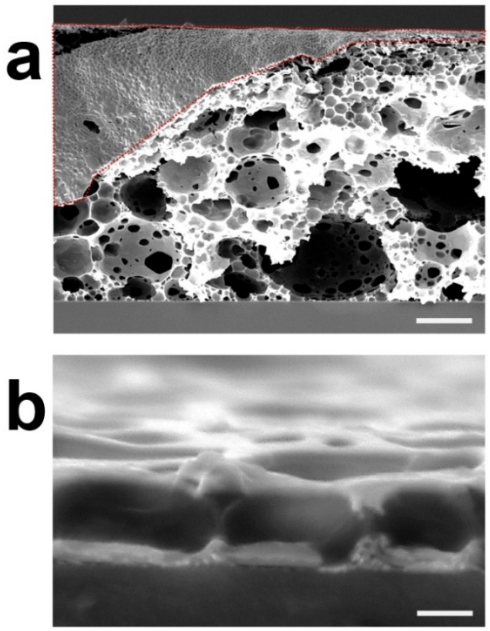

Figure 4. Representative cross-sectional SEM images of BF structures dip-coated from an emulsion containing modified 20 nm SiO_2 at different withdrawal speeds. a) Multilayer BF film produced at 1 mm/min consists of smaller pores on top of the film (region inside the dotted red curve) and larger pores underneath, and b) monolayer BF film dip-coated at 10, 50, 80, and 100 mm/min. The scale bars in figure a and b are 5 μm and 500 nm respectively.

droplets is controlled by two concomitant forces, which dictate whether the formed BFs are in a multilayer, monolayer, or unpatterned structure.[49] First, the temperature gradient in-

duced by evaporation creates a change in surface tension of the droplets. This leads to the droplets moving toward the substrate by thermo-capillary force (Marangoni convection force). Second, buoyancy force resulting from the viscosity of the solution, restrains the droplets by balancing the thermocapillary force. Besides these mentioned forces, in the context of our experimental setup, the fluid flow is an additional factor because of dip-coating being a dynamic process. The fluid dynamics in capillary and draining regime of dip-coating are illustrated in Figure 5.

At low dip-coating speed of 1 mm/min (capillary regime), evaporation happens at the same times as capillary feeding, thus Marangoni convection force is more dominant than in the draining regime due to evaporation (Figure 5a). This force then drives the droplets towards the solution-substrate interface. In the presented results, bigger droplets, penetrated deeper toward the substrate than the smaller ones did. This can be explained by the greater total interfacial energy of larger droplets,[54] leading to a larger absolute change in surface tension of these droplets in comparison to smaller ones. The cross-sectional SEM image of the films (Figure 4a) obtained in the capillary regime, where bigger pores were located underneath the surface layer of smaller pores, also complies with this hypothesis.

Higher dip-coating speeds of 10–100 mm/min produced monolayer BF films with a thickness of approximately 0.4–2 μm (Figure 4b). These films were likely created in the beginning of the draining regime, where thinner films are usually attained compared to those of the capillary regime.[42] In draining regime, the overall effective time used in film preparation is less, and neither the Marangoni convection nor the buoyancy force is dominant. Instead, high shear force present in this regime is the determinant, making the emulsion unstable by increasing the chance of droplets to coalesce. Thus, BF pores in this regime were significantly larger than those in the capillary regime (Figure 5b). Moreover, the gradual droplet growth with respect to increasing withdrawal speed in the draining regime can be attributed to the increased drying time due to a thicker entrained film, as observed previously in the work of Ogale *et al.*[55]

Care needs to be taken when comparing our dip-coating strategy to previous breath figure fabrication strategies reported in literature. For the latter, the drying atmosphere has typically been saturated with water. This extends the absolute drying time significantly in comparison to our experiments, where both the water and the $CHCl_3$ component evaporate faster when the films are withdrawn from the solution, thus making the system highly dynamic. Hence, a better analogue may be provided by spin-coating from solutions of water and water-miscible solvents, such as in the work of Park *et al.*[56] They observed a continuous increase of the breath figure diameters upon decreasing evaporation rate (decrease in spin-coating rate). In our case, the continuous pore diameter increase in the draining regime can thus be related to the longer evaporation time of thicker films. It is noteworthy, as pointed out by Vital *et al.*, that in the draining regime, the evaporation rate can depend on the experimental configuration.[57] However, both the tendencies of observing larger breath figure diameters in the draining regime than in the capillary regime, as well as the gradual increase of diameters as a function of increasing dip-coating rate in the draining regime, are agreeing with the trends previously observed using the spin coating technique. Overall, the dynamic nature of dip-coating can help creating diverse patterns in a much faster way than previously reported in the literature for emulsion methods.

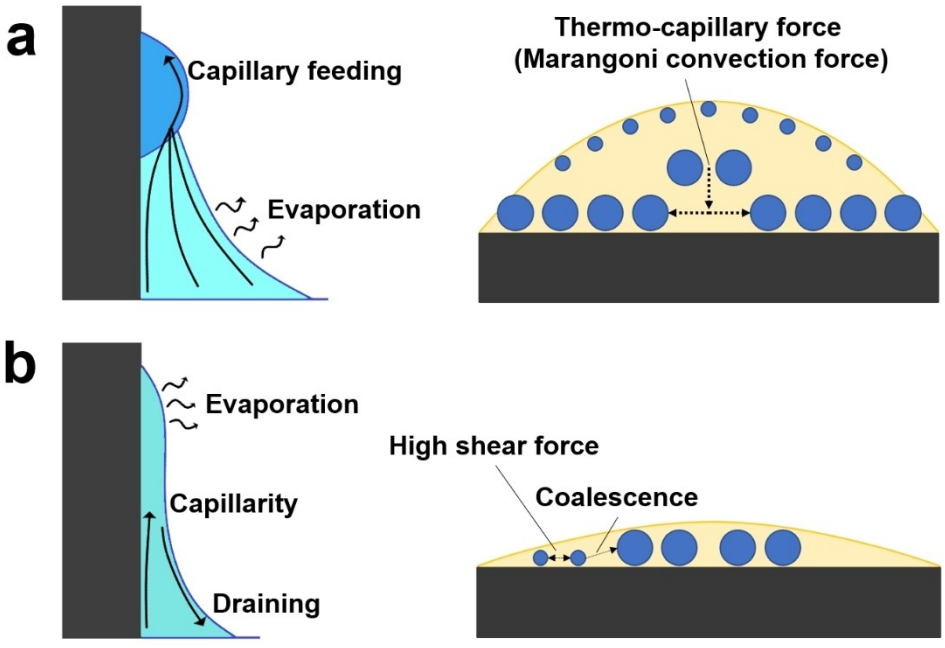

Figure 5. Schematic illustration of the fluid motion and the forces acting upon the water droplets in a) capillary regime and b) draining regime.

Effect of NP size

In the following section, we will discuss the impact of SiO_2 NP size on the development of the porous BF network by comparing the above used 20 nm NPs to ones of 500 nm diameter. Unlike the unmodified 20 nm NPs, the unmodified 500 nm NPs aggregated, and thus no stable emulsion could be created highlighting the need of surface coatings the NPs. Larger pristine SiO_2 NPs were previously reported to have inferior stability to that of smaller pristine NPs at low pH level, *i.e.* $pH < 6$[58] (the pH of our used chloroform solvent is approximately 4.5), not to mention their lower colloidal stability in solvents with low polarity.[59] However, when 500 nm SiO_2 NPs were hydrophobically modified, no aggregation was observed, and the emulsion retained its stability. BF films prepared from this emulsion surprisingly demonstrated a hierarchical structure containing both nano- and micrometer-size BFs simultaneously (Figure 6). The size of the nanopores, ranging from 250 to 284 nm in diameter, was in the same order as when using modified 20 nm SiO_2 NPs and did not vary significantly with increasing the withdrawal speed. Meanwhile, the microporous BFs grew with the dip-coating rates. Pores of ca. 12 μm were obtained at 1–10 mm/min, and 19 μm at 50–100 mm/min (Figure 7). It is worth mentioning that for

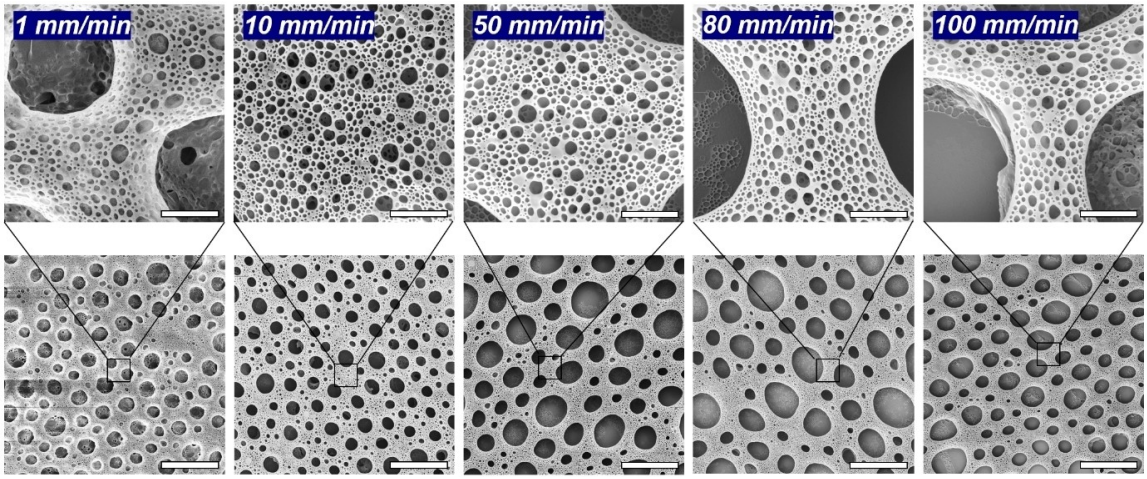

Figure 6. SEM images at two different magnifications of the films dip-coated from the emulsion containing hydrophobically treated 500 nm SiO_2 NPs. BF nanopores are shown in the above row, while BF microporous structures are shown below. The scale bars are 5 μm and 50 μm in the above and below rows of images respectively.

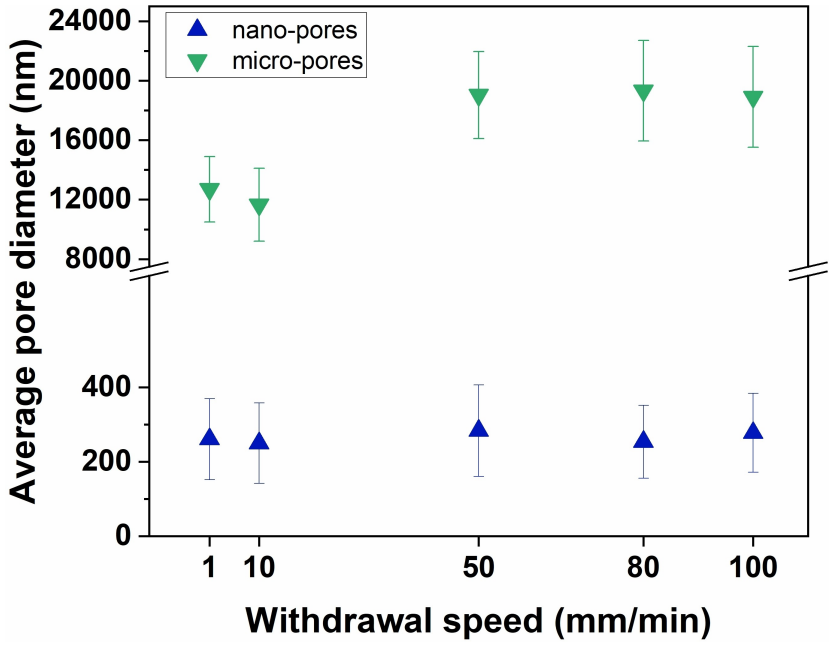

Figure 7. Relationship between withdrawal speed and average BF pore diameter of the films dip-coated from emulsion containing modified 500 nm SiO_2 NPs. The sizes of nano-size pores are illustrated by blue triangles and micro-size pores by green triangles.

Pickering emulsions the size of the dispersed droplets grows with the size of the stabilizing particles used,[60] which we did not observe for the nanopores. Yet, this does not explain the coexistence of the two different pore sizes. At the beginning of the emulsion formation, nanoscale droplets (ca. 250 nm) might be created as a result of the vigorous mixing step. The added 500 nm NP, which is much larger than the size of the original droplet, could not act as a stabilizer and in turn led to coalescence of these droplets into microscale ones. The steady growth of the nanoscale droplets would cease until their size reached the stable value (10–20 μm). The cross-sectional SEM images showing an enveloping layer of 500 nm NPs surrounding the microscale pore are described in Figure S5. This type of hierarchical porous network might potentially act as a model material for the mimicry of biologically important structures.

Evolution of BCP Nanostructures

To investigate the formed BCP patterns within the BF pores, AFM measurements were conducted to show the surface morphology of the films as a function of withdrawal speeds and NP sizes (Figure 8). For the films dip-coated from the emulsion containing 20 nm NPs, patterns of stripes (darker regions in AFM phase images) were observed at the lower speed regime of 1–10 mm/min. The morphology of films dip-coated at slow speeds from solution containing BCP but no water and NPs also represented stripes. Longer stripes were observed at 1 mm/min and shorter ones at 10 mm/min (Figure S6). These darker regions in all AFM images depict the softer phase in the film. In addition, the overall surface area of this phase is inferior to that of the brighter phase. Therefore, the striped pattern is expected to represent the P4VP block (which is the lower weight fraction block) in the BCP used. It is worth mentioning that the final morphology of the BCP in thin film will be closer to the bulk morphology if the solvent dissolves the two blocks equally.[61,62] Chloroform has been known as a nonselective solvent for PS-*b*-P4VP, and during the evaporation process when the film was withdrawn, chloroform distributed proportionally between the two blocks. Eventually, when the film was dried, its morphology behaved identically to that in equilibrium bulk state. Considering the weight fraction of our P4VP block, which is approximately 0.28, the striped surface morphology of the BCP likely stems from a cylindrical region.[63] Previous studies of dip-coated PS-*b*-P4VP thin films with similar volume fractions in chloroform also suggested the formation of cylindrical structures.[62,64–66] When faster dip-coating speeds were applied to the emulsion, *i.e.* 50–100 mm/min, a mixed pattern of horizontal and vertical cylinders developed. This changing in pattern might be analogous to the transition from long stripes (1 mm/min) to short stripes (10 mm/min) in the case of PS-*b*-P4VP films dip-coated from solutions without water and NPs. Meanwhile, at 50–100 mm/min, this solution produced "island-and-hole" features (Figure S6), due to incommensurability between the film thickness and the natural periodicity of the blocks, as reported in the work of Roland *et al.* using a similar setup and experimental parameters.[61]

The morphological evolution for the solution containing modified 500 nm NPs also displayed parallel cylinders at 1 mm/min. However, the transition in orientation happened much earlier, at 10 mm/min, and exclusively vertical cylinders appeared as dot patterns at 50–100 mm/min. Vertical cylinders in BCP thin films have been reported as a non-equilibrium phase at fast evaporation rates.[67,68] The appearance of bigger NPs likely imparted the mobility of the block, which together with the short time scale for film formation at high withdrawal speeds induced the kinetically trapped vertical cylinders.

In order to explain the realignment of cylinders during the dip-coating process, we propose a mechanism (Figure 9)

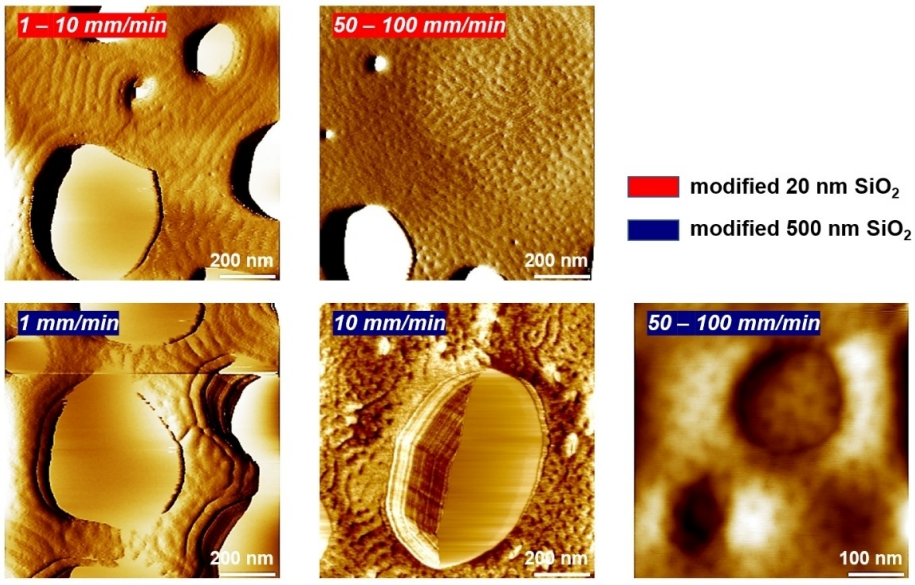

Figure 8. Representative AFM images of the BCP nanostructures in the BF films at different withdrawal speeds. All the images are phase images, except for the lower right one where a height image was obtained for better visualization.

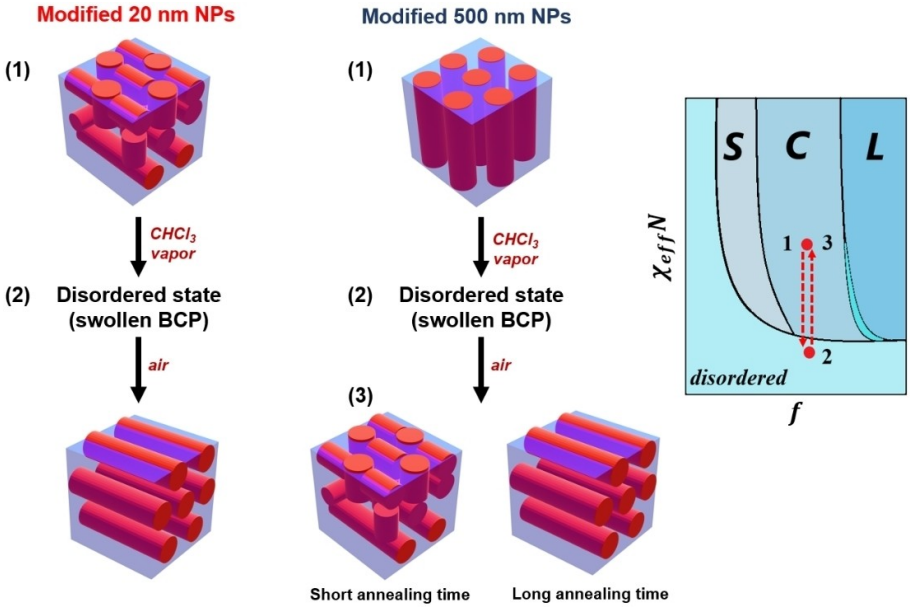

Figure 9. Schematic illustration of the reorientation of the BCP cylinders during dip-coating process of the emulsions containing 20 nm and 500 nm NPs. Letters S, C, L in the phase diagram are spherical, cylindrical, and lamellar phases respectively.

utilizing a previous model developed by Li *et al.* that described the effect of solvent vapor on the orientation of BCP cylinders.[69] When the blocks absorb solvent vapor, their interaction parameter can be described by equation (1):

$$\chi_{eff} \approx \varphi(\chi_{AB} + \chi_{A-S} - \chi_{B-S}) = \varphi(\chi_{AB} + \Delta\chi) \quad (1)$$

where χ_{eff} is the effective interaction parameter between the blocks, φ is the volume concentration of BCP in the solvent, χ_{AB}, χ_{A-S} and χ_{B-S} are the interaction parameters between the blocks, block A and solvent, block B and solvent, respectively.

For a nonselective solvent, the $\Delta\chi$ value can be assumed to be zero, thus $\chi_{eff} \approx \varphi\chi_{AB}$. When the speeds were lowered, the prolonged exposure to chloroform effectively reduced the volume concentration of the BCP ($\varphi < 1$) as well as the interaction parameter of the blocks (χ_{AB} decreased). Therefore, a decrease in χ_{eff} was expected. As illustrated in Figure 9, the segregation parameter of the BCP moved downward (point 1→ point 2), showing a transition from mix cylinders (emulsion containing modified 20 nm SiO_2) or vertical cylinders (emulsion containing modified 500 nm SiO_2) to a disordered phase, which was earlier reported to be the swollen BCP.[62] During the drying of the swollen BCP, the segregation value increased again (point 2→point 3) and had the tendency to support the unidirectional orientation of the cylinders. Because the water droplets acted as the template for the BCP phase separation, P4VP cylinders, which have a stronger affinity for water than PS, aligned parallel to the substrate, while PS phases with lower surface energy proceeded to the air–BCP interface. The degree of reorientation depends on the time scale of the withdrawal and also on the size of the immobilizing NPs.

Conclusion

In this work, a facile method to fabricate a hierarchical network of BF pores and BCP nanodomains has been demonstrated. By using the emulsion approach, BF pores can be formed without the presence of high humidity as precedentially required for the conventional BF technique. Moreover, the use of dip-coating, compared to drop-casting as a common method used in BF, has potential for industrial scalability as well as allows for a versatile thickness control, which can directly influence the structure of the BF pores *i.e.*, monolayer or multilayer. By varying the dip-coating speeds and the stabilizing NPs with different sizes and surface wettability, the BF pore sizes can range from 150 to 500 nm. Simultaneously, BCP nanopatterns of stripes and dots are created in the areas between the pores. By using larger NPs, we were able to produce an additional network of BF pores with microscale pores, creating a three-level hierarchical structure. Even though this approach produced pores with imperfect order, likely due to the dynamic nature of the dip-coating process, its implementation is significantly faster and easier than that of the conventional BF technique. Moreover, these structures resemble the structural heterogeneity of many biological materials, and the order of the pores is not essential for many applications like catalysis, that benefit from porous structures due to the enhanced surface area.

Most importantly, the interplay among BF and BCP evolutions, and different governing processes in both dip-coating and emulsion, were established in this model system. In the capillary regime of dip-coating, capillary action and evaporation play a key role in the formation of a multilayer BF structure, in which smaller pores were observed at the surface of the film. In the draining regime, on the other hand, a

monolayer was acquired, and larger pores appeared due to coalescence caused by high shear force. Lastly, the reorientation of the BCP nanostructure from dot (vertical cylinder) at high withdrawal speeds to stripe (parallel cylinder) at low speeds arose from the effective partial solvent annealing of the dip-coating process. This work is the first demonstration of three-level hierarchical pattern in emulsion-based BCP system. On top of that, considering the facile technique and the versatility of achieved BF and BCP patterns, more diverse patterns can be envisioned, which might be of great interest to templating, optoelectronic, and separation applications.

Experimental Section

Materials

PS-*b*-P4VP block copolymer (M_n of 25-*b*-10 kg/mol, Polymer Source), chloroform ($\geq$99.0%, Sigma Aldrich), trimethoxy(octadecyl)silane (TMOS, 90%, Sigma Aldrich), silica nanoparticles (monodisperse, non-porous, 20 nm and 500 nm, Sigma Aldrich), and glass substrates (microscope slides, VWR) were used as received. All experiments were performed at ambient conditions.

Emulsion Preparation and Thin Film Fabrication

PS-*b*-P4VP solution (10 mg/ml) was prepared by dissolving 0.05 g block copolymer in 5 ml chloroform and stirred overnight. For the emulsion containing unmodified silica, NPs of either 20 or 500 nm were then added to the BCP solution with the respective concentrations of 4 and 5 mg/ml and dispersed by a sonicator. For the emulsions containing modified silica, a prior step of modifying silica with TMOS was conducted, following a protocol reported elsewhere.[51] The final emulsion was created by adding 1 ml water to the BCP solution containing NPs, followed by a vigorous mixing step using a magnetic stirrer at 2500 rpm/min.

Glass substrates were cut into pieces of 1×1.5 cm and then cleaned with a Piranha solution, in which the volume ratio of sulfuric acid and hydrogen peroxide was 7:3 (*caution: Piranha solution is extremely corrosive and should be handled with care*). The substrates were immersed in Piranha solution for 20 min, then rinsed with deionized water, and dried with nitrogen gas.

The glass substrates were dip-coated from a vial containing the prepared emulsion using a KSV NIMA Single Vessel System (Biolin Scientific) dip-coater. The entire setup was placed on an anti-vibration platform, and the dip-coating process was conducted at an ambient RH of 36%. At the beginning of the dip-coating process, the substrates approached the emulsion at the rate of 25 mm/min and resided in the solution for 30 s. Withdrawal speeds to create BF films varied from 1 to 100 mm/min and the films were subsequently left to dry overnight in the dip-coating chamber.

Characterization of Modified Silica NPs and Emulsions

An attenuated total reflectance (ATR-IR) Perkin Elmer spectrometer was employed to characterize the chemical structure of the TMOS-modified silica NPs. The analysis measurement was performed in transmission mode with 32 scans and 4 cm^{-1} resolution.

Size measurements of the water droplets in the emulsions was carried out by a Zeta Sizer Nano ZS 90 system. The light scattering instrument has a 633 nm laser source and a backscattered angle of 173° was used for all measurements.

Thin Film Characterization

The morphology of BF films was characterized by a TESCAN MIRA 3 scanning electron microscope (TESCAN) using an accelerating voltage of 5 kV. Prior to the characterization, the samples were coated with a 5 nm conductive layer of Au/Pd (80/20) by sputtering. The pores size was analysed employing a home-built Python script, in which the SEM images were pre-processed and the border of the pores was defined using a Watershed function as described in Figure S1. Three different samples were used for each size calculation, and each SEM image contained roughly 1000–1500 pores.

The BCP nanostructure was imaged using a Multimode 8 atomic force microscope (Bruker) in tapping mode with non-contact AFM cantilevers (NCHV-A, Bruker). For better visualization of the patterns, the colour scale of the images was adjusted and flattened in the Nanoscope Analysis software (Bruker). Because the edge effect of the dip-coating process can lead to varied thickness of specifically the top and bottom parts of the films, all AFM measurements were carried out on the middle area of the films.

Contributions

Hoang M. Nguyen – Conceptualization, Main Investigation, Data Curation and Analysis, Visualization, Writing (Original Draft)

Ariane V. Mader – Preliminary Investigation, Writing (Review & Editing)

Swarnalok De – SEM Cross-Sectional Data Curation, Writing (Review & Editing)

Fevzihan Basarir – Writing (Review & Editing)

Jaana Vapaavuori – Supervision, Writing (Review & Editing)

Supporting Information Summary

The electronic Supporting Information contains a schematic illustration of the BF pore size calculation by Python, images of different BF emulsions and their corresponding dip-coated films, FTIR data showing the successful modification of SiO_2 NPs, DLS data of the water droplets measured from different emulsions, cross-sectional SEM images showing NPs surrounding a microscale pore, and AFM images of PS-*b*-P4VP thin films dip-coated from pure chloroform.

Acknowledgements

All the authors acknowledge the Academy of Finland SUPER-WEAR project (decision number: 322214) and European Research Council project "ModelCom" (decision number: 949648) for generous funding. This work made use of Aalto University Bioeconomy and RawMatters Facilities.

Conflict of Interest

There are no conflicts to declare.

Data Availability Statement

The data that support the findings of this study are available from the corresponding author upon reasonable request.

Keywords: breath figure · block copolymer · dip-coating · hierarchical porous structure · PS-b-P4VP

[1] P. Fratzl, R. Weinkamer, *Prog. Mater. Sci.* **2007**, *52*, 1263.
[2] W. A. Lopes, H. M. Jaeger, *Nature* **2001**, *414*, 735.
[3] Y. W. Kwon, J. Park, T. Kim, S. H. Kang, H. Kim, J. Shin, S. Jeon, S. W. Hong, *ACS Nano* **2016**, *10*, 4609.
[4] Q. Yang, S. Zhu, W. Peng, C. Yin, W. Wang, J. Gu, W. Zhang, J. Ma, T. Deng, C. Feng, D. Zhang, *ACS Nano* **2013**, *7*, 4911.
[5] L. Passoni, L. Criante, F. Fumagalli, F. Scotognella, G. Lanzani, F. Di Fonzo, *ACS Nano* **2014**, *8*, 12167.
[6] H. Sun, J. Zhu, D. Baumann, L. Peng, Y. Xu, I. Shakir, Y. Huang, X. Duan, *Nat. Rev. Mater.* **2019**, *4*, 45.
[7] Y. Zhang, X. Jing, Y. Cheng, T. Hu, M. Changgong, *Inorg. Chem. Front.* **2018**, *5*, 2798.
[8] S. Yin, Y. Zhang, J. Kong, C. Zou, C. M. Li, X. Lu, J. Ma, F. Y. C. Boey, X. Chen, *ACS Nano* **2011**, *5*, 3831.
[9] J. Ukkola, M. Lampimäki, O. Laitinen, T. Vainio, J. Kangasluoma, E. Siivola, T. Petäjä, H. Liimatainen, *J. Cleaner Prod.* **2021**, *310*, 127498.
[10] H. Wan, N. Wang, J. Yang, Y. Si, K. Chen, B. Ding, G. Sun, M. El-Newehy, S. S. Al-Deyab, J. Yu, *J. Colloid Interface Sci.* **2014**, *417*, 18.
[11] N. M. Vuong, N. D. Chinh, B. T. Huy, Y. I. Lee, *Sci. Rep.* **2016**, *6*, 1.
[12] R. Zhang, T. Zhou, L. Wang, T. Zhang, *ACS Appl. Mater. Interfaces* **2018**, *10*, 9765.
[13] A. K. Nayak, R. Ghosh, S. Santra, P. K. Guha, D. Pradhan, *Nanoscale* **2015**, *7*, 12460.
[14] A. Corma, U. Díaz, T. García, G. Sastre, A. Velty, *J. Am. Chem. Soc.* **2010**, *132*, 15011.
[15] M. Hartmann, A. G. Machoke, W. Schwieger, *Chem. Soc. Rev.* **2016**, *45*, 3313.
[16] C. M. A. Parlett, K. Wilson, A. F. Lee, *Chem. Soc. Rev.* **2013**, *42*, 3876.
[17] F. J. Martin-Martinez, K. Jin, D. López Barreiro, M. J. Buehler, *ACS Nano* **2018**, *12*, 7425.
[18] L. Mishnaevsky, M. Tsapatsis, *MRS Bull.* **2016**, *41*, 661.
[19] G. Widawski, M. Rawiso, B. François, *Nature* **1994**, *369*, 387.
[20] H. Bai, C. Du, A. Zhang, L. Li, *Angew. Chem. Int. Ed.* **2013**, *52*, 12240.
[21] M. Hernández-Guerrero, M. H. Stenzel, *Polym. Chem.* **2012**, *3*, 563.
[22] A. Zhang, H. Bai, L. Li, *Chem. Rev.* **2015**, *115*, 9801.
[23] P. Slepička, J. Siegel, M. Šlouf, D. Fajstavr, K. Fajstavrová, Z. Kolská, V. Švorčík, *Polymers (Basel).* **2022**, *14*, 4944.
[24] K. Oku, K. Ohno, D. Miyamoto, K. Ito, H. Yabu, K. Nakazawa, *Macromol. Biosci.* **2021**, *21*, 2100113.
[25] B. Chen, T. Wada, H. Yabu, *Adv. Mater. Interfaces* **2022**, *9*, 2101954.
[26] W. X. Zhang, L. S. Wan, X. L. Meng, J. W. Li, B. B. Ke, P. C. Chen, Z. K. Xu, *Soft Matter* **2011**, *7*, 4221.
[27] J. Bae, T. P. Russell, R. C. Hayward, *Angew. Chem. Int. Ed.* **2014**, *53*, 8240.
[28] Y. Wang, Z. Liu, Y. Huang, B. Han, G. Yang, *Langmuir* **2006**, *22*, 1928.
[29] H. T. Ham, I. J. Chung, Y. S. Choi, S. H. Lee, S. O. Kim, *J. Phys. Chem. B* **2006**, *110*, 13959.
[30] Y. Bo, S. Lei, W. Nangeng, L. Xiaohan, W. Limin, Z. Jian, *Macromolecules* **2008**, *41*, 9952.
[31] J. Liang, Y. Ma, H. Sun, W. Li, L. Wu, *J. Colloid Interface Sci.* **2013**, *409*, 80.
[32] W. Kasai, T. Kondo, *Macromol. Biosci.* **2004**, *4*, 17.
[33] Y. Ma, J. Liang, H. Sun, L. Wu, Y. Dang, Y. Wu, *Chem. A Eur. J.* **2012**, *18*, 526.
[34] A. Muñoz-Bonilla, E. Ibarboure, E. Papon, J. Rodriguez-Hernandez, *Langmuir* **2009**, *25*, 6493.
[35] E. Ji, V. Pellerin, F. Ehrenfeld, A. Laffore, A. Bousquet, L. Billon, *Chem. Commun.* **2017**, *53*, 1876.
[36] A. Aynard, L. Pessoni, L. Billon, *Polymer* **2020**, *210*, 123047.
[37] P. Escalé, M. Save, L. Billon, J. Ruokolainen, L. Rubatat, *Soft Matter* **2016**, *12*, 790.
[38] A. Bolognesi, F. Galeotti, U. Giovanella, F. Bertini, S. Yunus, *Langmuir* **2009**, *25*, 5333.
[39] W. Sun, Z. Shao, J. Ji, *Polymer* **2010**, *51*, 4169.
[40] H. Yuan, B. Yu, H. Cong, M. Chi, Y. Cheng, C. Lv, *Materials (Basel).* **2018**, *11*, 481.
[41] W. Sun, A. Ji, J. Shen, *Langmuir* **2008**, *24*, 11338.
[42] D. Grosso, *J. Mater. Chem.* **2011**, *21*, 17033.
[43] L. Landau, B. Levich, *Dyn. Curved Front.* **1988**, *17*, 141.
[44] C. H. Lee, A. J. Crosby, R. C. Hayward, T. Emrick, *ACS Appl. Mater. Interfaces* **2014**, *6*, 4850.
[45] K. Huang, Q. Cheng, H. Zhang, L. Lin, Q. Wang, *J. Mater. Res.* **2020**, *35*, 3210.
[46] B. Wu, M. Zhou, W. Zhang, Y. Liang, F. Li, G. Li, *RSC Adv.* **2017**, *7*, 24914.
[47] T. Luo, H. Bai, L. Li, *Langmuir* **2017**, *33*, 347.
[48] P. Escalé, L. Rubatat, C. Derail, M. Save, L. Billon, *Macromol. Rapid Commun.* **2011**, *32*, 1072.
[49] A. Chen, I. Blakey, A. K. Whittaker, H. Peng, *J. Polym. Sci. Part A* **2016**, *54*, 3721.
[50] Y. Xue, X. Li, J. Dong, *J. Colloid Interface Sci.* **2020**, *563*, 33.
[51] D. Sriramulu, E. L. Reed, M. Annamalai, T. V. Venkatesan, S. Valiyaveettil, *Sci. Rep.* **2016**, *6*, 1.
[52] G. Kaptay, *Colloids Surf. A* **2006**, *282–283*, 387.
[53] A. V Mader, Fabrication of Porous Hierarchical Multilevel Composite Thin Films by Combining Different Self-Assembly Processes, Aalto University, **2020**.
[54] A. Bolognesi, C. Mercogliano, S. Yunus, M. Civardi, D. Comoretto, A. Turturro, *Langmuir* **2005**, *21*, 3480.
[55] A. V. Limaye, R. D. Narhe, A. M. Dhote, S. B. Ogale, *Phys. Rev. Lett.* **1996**, *76*, 3762.
[56] M. S. Park, J. K. Kim, *Langmuir* **2004**, *20*, 5347.
[57] A. Vital, M. Vayer, T. Tillocher, R. Dussart, M. Boufnichel, C. Sinturel, *Appl. Surf. Sci.* **2017**, *393*, 127.
[58] M. Kobayashi, F. Juillerat, P. Galletto, P. Bowen, M. Borkovec, *Langmuir* **2005**, *21*, 5761.
[59] D. H. Lee, J. Jeong, S. W. Han, D. P. Kang, *J. Mater. Chem. A* **2014**, *2*, 17165.
[60] L. E. Low, S. P. Siva, Y. K. Ho, E. S. Chan, B. T. Tey, *Adv. Colloid Interface Sci.* **2020**, *277*, 102117.
[61] S. Roland, C. G. Gamys, J. Grosrenaud, S. Boissé, C. Pellerin, R. E. Prud'Homme, C. G. Bazuin, *Macromolecules* **2015**, *48*, 4823.
[62] E. B. Gowd, T. Koga, M. K. Endoh, K. Kumar, M. Stamm, *Soft Matter* **2014**, *10*, 7753.
[63] F. S. Bates, G. H. Fredrickson, *Annu. Rev. Phys. Chem.* **1990**, *41*, 525.
[64] B. Nandan, M. K. Vyas, M. Böhme, M. Stamm, *Macromolecules* **2010**, *43*, 2463.
[65] A. Sidorenko, I. Tokarev, S. Minko, M. Stamm, *J. Am. Chem. Soc.* **2003**, *125*, 12211.
[66] O. Seifarth, R. Krenek, I. Tokarev, Y. Burkov, A. Sidorenko, S. Minko, M. Stamm, D. Schmeißer, *Thin Solid Films* **2007**, *515*, 6552.
[67] S. Park, J. Y. Wang, B. Kim, W. Chen, T. P. Russell, *Macromolecules* **2007**, *40*, 9059.
[68] W. A. Phillip, M. A. Hillmyer, E. L. Cussler, *Macromolecules* **2010**, *43*, 7763.
[69] Y. Li, X. Wang, I. C. Sanchez, K. P. Johnston, P. F. Green, *J. Phys. Chem. B* **2007**, *111*, 16.

Submitted: March 2, 2023
Accepted: March 20, 2023